RSC Advances

ROYAL SOCIETY OF CHEMISTRY

www.rsc.org/advances

RSC Advances

PAPER

Self-assembly Mucoadhesive Nanofibers

P. Suvannasara[a], N. Praphairaksit[b] and N. Muangsin*[c]

Here, we proudly present an easy and stable one step to fabricate self-assembled nanofibers from modified chitosan. To obtain self-assembled, well-ordered nanofibers, we designed and synthesized stearic acid-4-carboxybenzenesulfonamide-*N*-trimethylchitosan by only re-dispersing the compound in distilled water at a concentration of 3.33 mg/mL. The self-assembled nanofibers had a diameter of 112.23 ± 11.96 nm with a narrow width distribution obtained through the aromatic stacking of 4-carboxybenzenesulfonamide, the hydrophobic effect of the stearic acid and the hydrogen bonding of the chitosan backbone. The intercoronal interaction of $-N^+(CH_3)_3$ provided an elongated axis of nanofibers. Furthermore, the ordered molecular organization of nanofibers led to high thermal stability and enhanced mucoadhesive properties compared to native chitosan, making the fabrication of these nanofibers a promising assembly method for drug delivery in acidic environment.

1. Introduction

Over the past few decades, nanofibers have been studied in medical science on the application of wound healing, tissue engineering, artificial organ components and drug delivery due to special properties mainly on their large surface area to volume ratio[1,2]. Several methods have been developed to fabrication nanofibers, including template synthesis[3,4], phase separation[5], electrospinning[6] and self-assembly[7,8]. The template synthesis is an effective route to make nanofibers or nanotubes using a nanoporous membrane as a template. On the other hand, the limitation of this method is it cannot make one-by-one continuous nanofibers and the membrane should be soluble so that it can be removed after synthesis to obtain nanofibers or nanotubes[9]. Although, the phase separation requires very minimal in term of equipment, the process takes relatively long period of time to transfer the solid polymer into the nanofibers consisting of dissolution, gelation, extraction using a different solvent, freezing, and drying[9]. Electrospinning have been recognized as an efficient technique to provide nanofibers. However, electrospinning requires a high voltage to create an electrically charged jet of polymer, provides broad range of fiber thickness, low mechanical properties of fiber meshes and does not control over 3D pore structure[10]. Polyethylene oxide was introduced to chitosan to fabricate ultrathin hybrid electrospun nanofibers with diameter ranging from 80-180 nm. However, it swelled rapidly in water and completely lost its fibrous structure within a few days[11]. Bhattarai et al. studied electrospinning to fabricate chitosan based nanofibers that can be a fiber size ~40 nm and the prolonged immersion of membrane in water up to 4 weeks[12]. However, triton X-100[TM] and DMSO were introduced into the solution as a surfactant and

cosolvent to reduce bead-like structure that embedded in the fibers and increase fiber yield, respectively. Geng et al. prepared electrospun homogeneous of nanofibers of pure chitosan dissolved in strongly aqueous acetic acid solution without addition of other solvent[13]. A bead free and more uniform nanofibers were formed by controlled the molecular weight of chitosan at 106,000 g/mol at 7% concentration, dissolved in 90% aqueous acetic acid solution.

The macromolecular self-assembly of nanomaterials into high-order and stable structures has become an attractive strategy with preprogrammed non-covalend bonds[14]. Unlike electrospinning, self-assembly provides to autonomous organization of molecules into patterns or structures without human intervention and produce much thinner nanofibers only several nanometers in diameter[9]. Peptide amphiphiles (PAs), a new class of biomaterials, were designed to understand the self-assembly of amphiphiles and the chemical complexity of peptides. PAs include a class of molecules that form highly hydrophobic chains. These chains can attach to hydrophilic peptides to create amphiphilic hybrid molecules. Niece et al. prepared self-assembly combining two bioactive PA molecules into nanofibers revealed fibers with approximately 7 nm in diameter and several micrometers long[15]. Hartgerink et al. prepared PAs of mono-alkyl chains attached via the *N*-terminus without proline residues, representing a highly flexible method for achieving chemical functionality in one-dimensional nanostructures[16]. These PAs can self-assemble into nanofibrous cylindrical micelles with almost equivalent tolerant properties of an amino acid. Paramonov et al. studied the role of hydrogen bonding and amphiphilic packing in the self-assembly of a series of 26 PA derivatives[17]. Due to the ease of synthesis and the chemically tolerant nature of self-assembled PAs, simulating PAs is of great interest. Nevertheless, self-assembled PAs are unstable at physiological pH unless the pH is controlled by the

addition of a multivalent cation or by internally cross-linking the PA through covalent bonds[18].

Chitosan, another natural biomaterial, was chosen herein as a molecular model because its polymer chain is biocompatible, stable, non-toxic to human health, mucoadhesive and flexible. Chitosan has been extensively employed in biomedical materials, especially for drug delivery applications[19]. In addition, chitosan is a unique natural alkalescent polysaccharide that contains a double helix structure[20]. Chitosan is easily prepared from chitin and has a reactive amino group that can be chemically modified and can carry a positive charge during reactions. Moreover, chitosan can be prepared into nanofibers without the need to control temperature and pH or to add a co-assembling molecule.

To construct the nanofibers, we designed and synthesized stearic acid-4-carboxybenzenesulfonamide-*N*-trimethylchitosan (SA-4-CBS-TMC) to induce the self-assembly of well-ordered nanofibers in distilled water. The nanofiber assembly relied on a balance between the hydrophobic effect of the stearic acid (SA), the aromatic stacking of 4-carboxybenzenesulfonamide (4-CBS), the electrostatic interactions of $-N^+(CH_3)_3$ and the hydrogen bonding of the chitosan backbone. The driving force for the hydrophobic packing of the SA chains in an aqueous environment allows the specific presentation of 4-CBS and $-N^+(CH_3)_3$ hydrophilic signals on the surface of the assembled nanofibers, leading to an enhancement of helical structure. The great improvement derived from utilizing SA-4-CBS-TMC is that the structural features of the final assembly can be finely, easily and readily tuned by modulating only the factors pertaining to the re-dispersed concentration independent of the assembling environment (e.g., pH, co-assembling molecule and temperature) while providing a narrow size distribution.

2. Experimental section

2.1 Materials

Chitosan with a weight average molecular weight, M_w, of 500 kDa was provided by Seafresh Chitosan (Lab.) Co., Ltd. in Thailand. The degree of deacetylation of chitosan was determined to be 81 % by ^{1}H-NMR. 4-CBS, methyl iodide (CH_3I), *N*-methyl pyrolidone (NMP), 1-ethyl-3-(3-dimethylaminopropyl)carbodiimide (EDAC), *N*-hydroxylsucci mide (NHS), SA and mucin (type II) from porcine were purchased from Aldrich Co., USA and used without purification. A cellulose dialysis tubing (Membrane Filtration Products, Inc., USA) with molecular weight cut-off 12-14 kDa was used to purify all modified chitosan. All other chemicals were obtained commercially as reagent grade and used as supplied.

2.2 Synthesis of *N*-trimethyl chitosan chloride (TMC)

TMC was synthesized according to previously method[21]. Briefly, the mixture of 100 mL of a 1% (w/v) of chitosan in 1% (v/v) acetic acid solution, 5 ml of 15% (w/v) aqueous sodium hydroxide and 30 ml of CH_3I in 30 mL of NMP was heated at a temperature 60 C° for 45 min. The product was precipitated with 80 % (v/v) ethanol and isolated by centrifugation (12,000 rpm, 5 min, RT). After washing with ethanol, the product was dissolved in 40 mL of 5% (w/v) aqueous sodium chloride solution to exchange the iodide ion with a chloride ion. The polymer was precipitated with ethanol and isolated by centrifugation (12,000 rpm, 5 min, RT). This product was dissolved in 40 mL distilled water, precipitated with ethanol to remove the remaining sodium chloride from material, lyophilized at -44 °C and 0.01 mbar and stored at 4 °C before use. Yield: 92.54%.

^{1}H-NMR (400 MHz, D_2O/CF_3COOH, δ (ppm)): 3.95-3.20, (m, 5H, H3-H6), 3.15 (s, 3H, 6-OCH_3), 2.90 (s, 3H, 3-OCH_3), 2.77 (s, 1H, H2), 2.64 (m, 9H, $N^+(CH_3)_3$), 2.45 (m, 6H, $N(CH_3)_2$), 2.30 (m, 3H, NHCH_3) and 1.65 (s, 3H, NHCOCH_3). EA analysis: C, 28.02%; H, 5.24%; N, 4.26%.

2.3 Synthesis of 4-carboxybenzenesulfonamide-*N*-trimethyl chitosan (4-CBS-TMC)

TMC was fully dissolved (0.01 g/mL) in 1% (v/v) acetic acid at room temperature overnight to perform 100 ml TMC solution, and then 4-CBS (0.2 g, 9.94 mmol), EDAC (0.24 g, 1.25 mmol), and NHS (0.24 g, 1.42 mmol) were added to the mixture. The reaction mixture was refluxed for 12 h to form the 4-CBS-TMC. Excess EDAC and NHS were removed by adding 1 M HCl and then adding 1 N NaOH to precipitate the mixture. The precipitated mixture was dialyzed in ethanol to removed free acetic acid, HCl, NaOH, *o*-acylurea and unreacted 4-CBS for 1 day. The reaction mixture was then centrifuged, washed with distilled water and freeze dried to being lyophilized at -44 °C and 0.01 mbar. Yield: 89.35%. ^{1}H-NMR (400 MHz, D_2O/CF_3COOH, δ (ppm)): 7.97 (d, 2H, J = 8.0 Hz, Ph), 7.78 (d, 2H, J = 8.0 Hz, Ph), 4.10-3.38, (m, 5H, H3-H6), 3.33 (s, 3H, 6-OCH_3), 3.10 (s, 3H, 3-OCH_3), 2.94 (s, 1H, H2), 2.82 (m, 9H, $N^+(CH_3)_3$), 2.63 (m, 6H, $N(CH_3)_2$), 2.43 (m, 3H, NHCH_3) and 1.84 (s, 3H, NHCOCH_3). EA analysis: C, 41.05%; H, 8.06%; N, 6.13%.

2.4 Synthesis and self-assembly of SA-4-CBS-TMC Nanofiber

4-CBS-TMC was fully dissolved (0.01 g/mL) in 1% (v/v) acetic acid at room temperature overnight to provide 20 ml TMC-4-CBS solution. SA (0.1 g, 0.35 mmol), EDAC (0.34 g, 1.76 mmol), and NHS (0.20 g, 1.76 mmol) were dissolved in 7 ml of an ethanol/acetone mixture (ethanol/acetone = 2/5 (v/v)) and then heated at 60 °C for 1 h. The solution was added into the 4-CBS-TMC solution, followed by stirred and refluxed for another 24 h as schematically summarized in Fig. S1. Finally, the reaction solution was dialyzed against distilled water for 1 day using a dialysis membrane to remove excess EDAC and NHS and lyophilized at -44 °C and 0.01 mbar. Then the lyophilized product was further purified with ethanol to remove byproduct. The product SA-4-CBS-TMC was re-dispersed in distilled water and vortexed to form nanofiber. Yield: 85.94%. EA analysis: C, 46.90%; H, 8.04%; N, 5.11%.

2.5 Determination of the degree of quaternization (%DQ) and degree of 4-CBS substitution (%DS$_{4-CBS}$)

The degree of quaternization and degree of 4-CBS substitution of the TMC were determined by ^{1}H-NMR spectra using 2% (v/v) trifluoroacetic acid (CF_3COOH) in D_2O were calculated using eq (1) and (2), respectively.

$$\% DQ = \left[\frac{I_{(CH_3)_3}}{I_{(H3\text{-}H6)}} \times \frac{5}{9} \right] \times 100 \ldots\ldots(1)$$

$$\% DS_{4-CBS} = \left[\frac{I_{(SO_2NH_2)}}{I_{(H3\text{-}H6)}} \times \frac{5}{2} \right] \times 100 \ldots\ldots(2)$$

where $I_{(CH_3)_3}$ is the integral of the trimethyl amino group (quaternary amino) protons of TMC at 2.64 ppm, $I_{(SO_2NH_2)}$ is the integral of the benzene ring of 4-CBS-TMC protons at 7.97 ppm and $I_{(H36)}$ is the integral of the H3-H6 protons of chitosan or 4-CBS-TMC at 3.95-3.20 ppm or 4.10-3.38 ppm, respectively.

2.6 Characterization

The lyophilized sample of TMC, 4-CBS-TMC and SA-4-CBS-TMC were characterized by ^{1}H NMR, FT-IR, X-ray diffraction (XRD) and TGA. The ^{1}H NMR spectra was determined by Varian 400 MHz spectrometer using 2% (v/v) trifluoroacetic acid (CF_3COOH) in D_2O at 300 K, pulse accumulating of 64 scans. FT-IR spectra were recorded on Nicolet 6700 in the region from 4000 cm^{-1} to 400 cm^{-1}. Carbon, hydrogen and nitrogen elemental analysis were performed on a CHNS/O analyzer (Perkin Elmer, PE2400 Series II). XRD was performed on a Rigaku X-ray diffractometer Dmax 2200 Ultima at room temperature with a speed scan of 5°/min using CuKα radiation (λ=1.5405 A°, 40 kV, 30 mA) to study polymers'aggregation and determined % crystallnity. Thermogravimetric analysis (TGA) was performed on a PerkinElmer Pyris Diamond TG/DTA machine to study thermal stability. About 5 mg of lyophilized samples dried in vacuum overnight were put into aluminium pan and measured under a nitrogen flow at a rate of 25 mL/min. The mass of aluminium pan was continuously recorded as a function of temperature. The morphology and surface appearance of the different concentration on self-assembly of SA-4-CBS-TMC particles were examined by scanning electron microscopy. The self-assembly of SA-4-CBS-TMC particles were prepared by redispersed in distilled water with a concentration of 0.33, 0.67, 3.33 and 13.33 mg/mL and then vortexed for 2 h. Each sample solution was dropped on stub using double-sided carbon adhesive tape, dried in desiccator overnight and coated with gold–palladium. Coating was achieved at 18 mA for at least 4 min. The scanning was performed under high vacuum at an ambient temperature with a beam voltage of 20 kV. The swelling degree of dried chitosan and 4-CBS-TMC films were observed the change in the diameter of the films as previous described[18]. Each polymer (1 g) was dissolved in 50 mL of 1% (v/v) acetic acid, and the solution was then poured into a plastic plate (8 cm × 10 cm) and left at ambient conditions until dry. The dried films were cut into 6.0 mm diameter discs using a paper punch. The swelling ratios were measured at particular predetermined time points after immersion in the respective solutions, distilled water, simulated gastric fluid (SGF, pH 1.2), 0.1 N simulated duodenum buffer (SDF, pH 4.0), 0.1 N phosphate buffer (PB, pH 5.5), simulated jejunum fluid (SJF, pH 6.4) and simulated ileum fluid (SIF, pH 7.4) at room temperature, and were evaluated by measuring the change in the diameter of the flat discs using a micrometer scale. The swelling ratio (S_w) of each film was determined ($S_w = (D_t - D_0)/D_0 \times 100$), where D_t is the film diameter at time t and D_0 is the initial film diameter.

2.7 Determination of the mucoadhesiveness

The mucoadhesive properties of chitosan, TMC, 4-CBS-TMC and SA-4-CBS-TMC were determined based on the viscometric changes of porcine gastric mucin and polymers in both SGF and PB buffer as previously reported[22] at 37 °C on a Brookfield (Model DV-II) viscometer. Briefly, dried mucin was hydrated with buffer by gentle stirring for 3 h at 25 °C to yield 20% (w/v) dispersion. 4-CBS-TMC was dissolved in 10% (v/v) acetic acid to yield 4% (w/v) 4-CBS-TMC solutions that was then diluted by a buffer to yield the

respectively 1% (w/v) 4-CBS-TMC solution. The viscosities of the 15% (w/v) mucin-1% (w/v) polymer mixtures were mixed with SGF or PB for 24 h at 37 °C and then measured. In case of SA-4-CBS-TMC, it was only re-dispersed in buffer. The mucoadhesive properties of the conjugates in SGF were compared with that in the PB buffer using same method. The viscosity coefficient was then determined by Eq. (3) as follows:

$$\eta_t = \eta_m + \eta_p + \eta_b \ldots\ldots(3)$$

where η_t is the viscosity coefficient of the system, η_m and η_p are the individual viscosity coefficients of the mucin and polymer, respectively, and η_b is the viscosity component due to the mucoadhesive. All assays were performed in triplicate with the results shown as the mean $\pm$ one standard deviation (SD).

2.8 Statistical analysis

All measurements were performed in triplicate in each experiment with the results presented as the mean $\pm$ 1 SD. Statistical analysis was performed by one-way ANOVA using Microsoft Excel (Microsoft Corporation) with $P < 0.05$ considered to indicate statistical significance.

3. Results and discussion

To well understand the synthesis of SA-4-CBS-TMC, the covalent attachment of 4-CBS and SA to TMC was achieved via coupling the carboxylic acid group (–COOH) of 4-CBS and SA to the primary amine groups (–NH_2) of TMC using EDAC (Fig. S1). The lyophilized product, SA-4-CBS-TMC, appeared as a white, odorless fibrous polymer. Lyophilized fibrous polymers were characterized using ^{1}H NMR (Fig. S2) and FT-IR (Fig. S3). ^{1}H NMR analysis showed the degree of TMC quaternization at 26.84% and the degree of substitution of 4-CBS on TMC at 7.78%. FT-IR spectrum had the presence of amide band I and II at 1643 cm^{-1} at 1565 cm^{-1}, respectively, strong intensity peaks of C-H aliphatic stretching of SA substituent at 2916 cm^{-1} and 2874 cm^{-1}, and methyl group bending of long chain SA on TMC backbone. However, no absorption peak of carboxyl groups of SA (1703 cm^{-1}) was found in SA-4-CBS-TMC spectrum, indicating that there was no unreacted SA in product. The XRD diffractogram (Fig. S4) revealed two primary diffraction regions, one at approximately 6°-10° (2θ) and another at approximately 19°-24° (2θ). The peak in the low angle region is relatively strong and sharp, indicating the highly substituted molecular order of SA on the TMC backbone. The second peak found at the higher angle was low and broad due to the steric effects of 4-CBS on the backbone. The thermal stability of SA-4-CBS-TMC was confirmed by TGA (Fig. S5), which showed a weight loss of the backbone at higher temperatures (478 °C) compared to TMC (303 °C) and TMC-4-CBS (335 °C). This result indicates that SA-4-CBS-TMC had a more crystalline XRD pattern, leading to high thermal stability and resistance to degradation.

3.1 Effect of the concentration on self-assembly of SA-4-CBS-TMC

To illustrate the self-assembly of the synthetic polymer, we aimed to reduce the complexity of the self-assembled PA, such as instability and denaturing under harsh conditions. The molecular design of the SA-4-CBS-TMC nanofibers is shown in Fig. 1. The PAs were designed with long alkyl hydrophobic blocks on one end

of hydrophilic peptide sequences, creating an amphiphilic hybrid molecule. The self-assembly of non-amphiphiles is difficult to induce because the property variation between the core and the end groups may not be large enough to induce a phase separation[23]. Fig. 1 displays the chemical structure of one SA-4-CBS-TMC molecule, incorporating the four key structural features: the 4-CBS substituent, $-N^+(CH_3)_3$ of the quaternized chitosan, SA hydrophobic tail and the chitosan backbone. The first key component, the aromatic 4-CBS substituent, induced π-π aromatic stacking interactions between small aromatic rings and allowed the formation of well-ordered nanofibers. These interactions provided discrete nanostructures due to the extremely rigid characteristic of the nanofibers when re-dispersed in distilled water. The second key component, the quaternized chitosan $-N^+(CH_3)_3$, enhanced the nanofiber solubility in water without altering the pH. Normally, charges can be induced in PA amino acids by changing the pH and the concentration of electrolyte in the solution[24]. Therefore, pH is a critical factor for generating successful self-assembled nanofibers. The third key element was the inclusion of various hydrophobic tails with different alkyl lengths, such as palmitic acid[23], phospholipids[15] and SA[25], to assemble the nanofibers. SA served one of the most important roles for designing this molecular feature. SA contains hydrophobic regions to control the self-assembly of amphiphiles by shielding the amphiphiles from water to create 4-CBS and $-N^+(CH_3)_3$ signals on the nanofiber periphery. The last key component, the chitosan backbone, formed intramolecular hydrogen bonds, which led to further enhanced horizontal molecular packing at both very low and high polymer dispersed concentrations. Therefore, intermolecular hydrogen bonding caused the connection of SA-4-CBS-TMC nanofibers, one factor for molecular packing. Utilizing these key factors, nanofibers were fabricated in water. The hydrophobic core of the SA substitution was buried within the structure such that it did not contact water, whereas the hydrophilic segments, such as $-N^+(CH_3)_3$ of the chitosan backbone and the 4-CBS substituent, surrounded the SA core and resided adjacent to the water phase. The driving forces of aromatic 4-CBS stacking, hydrogen bonding along the chitosan backbone, the hydrophobic interactions of the alkyl SA tails and the electrostatic repulsion of $-N^+(CH_3)_3$ enhanced the helical structure formation and facilitated the self-assembly of SA-4-CBS-TMC nanofibers. Self-assembly of chitosan derivatives based amphiphile exhibited the helical structure such as octanoyl-chitosan-polyethylene glycol monomethyl ether (acylChitoMPEG) which was determined by SAXS[26]. The aromatic 4-CBS stacking, chitosan backbone and alkyl SA tails were attractive forces that promoted the aggregation of SA-4-CBS-TMC, whereas the $-N^+(CH_3)_3$ was the charged component that promoted the dissociation of SA-4-CBS-TMC. As the molecular-level packing progressed, which depended on a delicate balance of energy contribution, the morphological and structural features, including length, packing density and order of surface fibers, were revealed.

Fig. 1 The molecular (a) structure of SA-4-CBS-TMC and (b) design of SA-4-CBS-TMC nanofibers.

Factors that can control molecular structure assembly include pH, solvents, co-assembly molecules, temperature and re-dispersed concentration. Self-assembly induced through pH change is unstable at physiological pH unless an internal cross-link with a co-assembly molecule forms an electrostatic stable molecule containing the opposite charge. A class of PA-assembled nanofibers has been prepared under physiological conditions in the presence of polyvalent metal ions, such as Mg^{2+}, Ca^{2+}, Ba^{2+}, Cu^{2+}, Zn^{2+} and Gd^{3+}. However, these various divalent metal ions were difficult to prepare[19]. Temperature is also an important factor that affects the tolerance of protein and peptides in self-assembling.

Fig. 2 (a) A schematic phase diagram of SA-4-CBS-TMC assemblies, which are dependent on concentration in distilled water, ranging from 0.33 to 13.33 mg/mL. (b) The formation stages of SA-4-CBS-TMC particles dependent on re-dispersion in distilled water.

In this study, for the self-assembly of SA-4-CBS-TMC molecules, re-dispersion concentrations ranging from 0.33 to 13.33 mg/mL in distilled water were first considered to control the fabrication of nanofibers (Fig. 2a). As shown in Fig. 2b, in the early stages, while the SA-4-CBS-TMC particles were dispersed in distilled water, the peripheral chitosan backbone was separated. Next, the particles gradually swelled, resulting in aggregation due to the random walk process[27], and became primitively self-assembled. This process allowed an alteration in self-assembly structure in response to changing the concentration of SA-4-CBS-TMC in distilled water. The final nanofiber shape, size and self-assembled stability expressed an optimum thermodynamic state, which was characterized by a combination of factors, such as chain stretching, interfacial tension and intercoronal chain interaction[28]. The excellent long term stability of various morphologies dispersed in distilled water could be determined by re-observation by SEM. Although the self-assembly of a spherical geometry was quite general, other morphologies, such as short fibrous bundles, nanofibers, hyperbranched structures and films, were observed at different re-dispersion concentrations. All of morphologies were not change in shape and size over time.

3.1.1 Spherical shapes and short fibrous bundles

At a low concentration (0.33 mg/mL), the morphologies of SA-4-CBS-TMC structures included spherical shapes and short fibrous bundles (Fig. 3). The relative stability of the various possible packing self-assemblies was believed to be primarily controlled by the balance of three energies: chain stretching, interfacial tension and intercoronal chain interactions. When the concentration was low, the amount of SA-4-CBS-TMC was too low to provide the high intercoronal chain repulsion of $-N^+(CH_3)_3$ on the surface. The SA-4-CBS-TMC structure was determined by a delicate balance of forces operating at the interfacial region of the 4-CBS and $-N^+(CH_3)_3$ groups and within the hydrophobic core of aggregated SA, inducing a spherical shape (Fig. 3a). The spherical shape resulted in the minimum total free energy and therefore was the first morphology that was assumed by the structure. However, the formation of SA-4-CBS-TMC into spheres could not continue indefinitely because the stretching energy due to the entropy of SA became limited as the radius of the sphere increased during core formation. Consequently, the high stretching energy would begin to induce short fibrous bundles instead of spheres to reduce the thermodynamic penalty of chain stretching (Fig. 3b).

Fig. 3 The morphologies of SA-4-CBS-TMC at low concentration (0.33 mg/mL): (a) spherical shapes, (b) fibrous bundles, (c) fibrous bundle merge and (d) the proposed self-assembly of fibrous bundles.

Several short fibrous chains linked themselves along the horizontal axis to create a fibrous bundle (Fig. 3b). The proposed self-assembly process of the fibrous bundle structures is shown in Fig. 3d. The quaternary amino group of the chitosan backbone and the sulfonamide group of 4-CBS provided cation-dipole interaction. Moreover, the stacking force of 4-CBS prolonged the length of the bundles. Nevertheless, only short fibrous bundles occurred due to the

minimal amount of SA-4-CBS-TMC. The SEM image (Fig. 3c) shows the merging of the fibrous bundles, which was dependent on the interfacial tension force. The bundles merged to reduce the interfacial tension, creating a stable SA-4-CBS-TMC molecule.

3.1.2 Tree-like morphology or hyperbranced structure

The tree-like morphology, or the hyperbranched structure shown in Fig. 4, was able to be formed at a concentration of 0.67 mg/mL. The formation of the structure began as the aggregation of many nuclei (Fig. 4a), a state of lower free energy[29]. The concept of diffusion-limited aggregation (DLA), or the irreversible aggregation of small particles into clusters, has been previously developed[30]. The DLA concept received significant attention because it was a fundamental model for pattern growth and provided a basic understanding of complex aggregate formation of different shapes[31]. The model assumed that particles originate far from a developing immobile structure and undergo a random walk in their surrounding space. The particles stick to an existing structure when encountered. Therefore, the aggregated nuclei of SM-4-CBS-TMC became part of the primitive self-assembly that led to the formation of extremely complicated multi-branches (Fig. 4b). These branches grew from the central nucleus and were composed of short helical SA-4-CBS-TMC nanofibers with a width on the order of ~100 nm (Fig. 4c). Moreover, these branches repelled each other due to the repulsive positive charge of the $-N^+(CH_3)_3$ group. Generally, a hyperbranched structure formed and grew rapidly at the ends of the self-assembly rather than from other perimeter sites because the perimeter sites near the center were occluded[32].

Fig. 4 The morphologies of SA-4-CBS-TMC at high concentration (0.67 mg/mL): the (a) initial nucleus, (b) central nucleus, (c) short helical nanofibers of ~100 nm and (d) proposed self-assembly of hyperbranched structures.

The proposed hyperbranched self-assembly feature with a tip-splitting head is shown in Fig. 4d, which illustrates the formation of distinct borders. The angles between the main and side branches, considered from the center outward, do not have fixed values. The widths of the branches were much narrower compared to the total length of each branch. Moreover, the branches were formed with a uniform width. When a branch reached a certain width, it split to generate new branches, and both the parent branch and the new branches continued to proliferate. This pattern generated an approximately geometrical ellipse, with a largest diameter of approximately 60 μm. Thus hyperbranched self-assembly of SM-4-CBS-TMC at a high concentration was successfully prepared.

3.1.3 Nanofiber formations

At a concentration of 3.33 mg/mL, nanofiber formations were observed (Fig. 5). The SEM micrograph of SA-4-CBS-TMC (Fig. 5b) revealed a nanofiber cross-section with a convex spherical surface due to helical molecular packing. The aromatic 4-CBS substituents, creating π-π aromatic stacking, and the amino groups of the chitosan backbone, governing hydrogen bonding, exposed active functional groups on the surface of the fibers. As the SA aliphatic tails were aggregated, they repelled the distilled water and induced formation of the helix. Methylation of $-N^+(CH_3)_3$, which formed an intercoronal interaction, induced elongation of the nanofiber axis. Moreover, the SEM micrographs depicted connected horizontal SA-4-CBS-TMC nanofibers (Fig. 5c), which was partly due to hydrogen

bonding of the amino groups of the chitosan backbone and the sulfonamide groups of the 4-CBS substituent.

Fig. 5 Morphologies of SA-4-CBS-TMC at high concentration (3.33 mg/mL). (a) Elongated nanofibers, (b) a cross-section of nanofibers (c) connected horizontal nanofibers are depicted, and (d) the histogram of SA-4-CBS-TMC nanofiber widths measured from SEM images.

The orientation of hydrogen bonding was important in the formation of nanofibers. A minimum number of hydrogen bonds was necessary for the formation of the SA-4-CBS-TMC nanofibers. Due to the low number of hydrogen bonds, the energy of the remaining hydrogen bonds was not enough to induce nanofiber aggregation. This phenomenon was only able to form self-assembled spheres. Therefore, the disruption of the hydrogen bonds of the amino groups on the chitosan backbone by $-N^+(CH_3)_3$ substituents was able to prevent SA-4-CBS-TMC from donating hydrogen bonds. Considering the 4-CBS substituent as a short aromatic chain, 4-CBS was further from the SA nanofiber core compared to the amino groups of the chitosan backbone. 4-CBS was also less tightly governed by hydrogen bonding. Another class of peptide nanostructures has been previously reported involving the use of short aromatic peptides to form well-ordered nanostructures. Previous studies reported that the formation of closed-caged nanospheres was most likely due to geometrically restricted interactions between aromatic moieties, such as diphenylglycine polypeptide. A simpler analogue, the Alzheimer's β-amyloid diphenylalanine structural motif, is a flexible and less restricted peptide that forms discrete nanotubes due to the stacking of aromatic residues[33]. Therefore, the partial elimination of the amino group of the chitosan backbone and a less restricted aromatic interaction were critical for the formation of elongated nanofibers (Fig. 5a). The peak of the histogram of SA-4-CBS-TMC nanofiber widths (Fig. 5d) at these concentrations, derived from SEM images, was determined to be 112.23 ± 11.96 nm with a narrow width distribution. Haider et al. attempt to fabricate electrospun chitosan nanofibers with their highly aligned narrow diameter ~130 nm; however, the chemical neutralization of ammonium into amine was needed for the preparation to increase stability in aqueous medium[34]. Although Stendahl et al. fabricated self-assembly of PA ($C_{16}A_4G_3S(P)KGE$-COOH) into gel-forming networks of cylindrical aggregates with approximate diameter narrower than SA-4-CBS-TMC nanofibers ~15 fold, lengths that frequently exceed one micrometer and the concentration, electronic structure, and hydration of counterions significantly influence self-assembly and mechanical properties[35]. Therefore, these re-dispersion concentrations are an easy and stable technique to create the appropriate ratio to form well-defined, self-assembled nanofibers with stable structure for nanotechnology applications.

3.1.4 Thin films

At very high concentration (13.33 mg/mL), the space between polymeric units was very limited (Fig. S6). The concentration promoted growth onto functionalized interfaces. The nanofibers did not have enough space to permit facile growth. Therefore, the high polymer content induced aggregation into thin films.

3.2 Swelling behavior

The swelling behavior indicates the relative ease and speed of liquid penetration into a polymer matrix, which is an essential step

and important influence on the kinetics of the drug release process. In addition, the swelling behavior of mucoadhesive polymers has a strong influence on their adhesive properties, water-uptake and stability[36]. A rapid swelling behavior may improve the inter-diffusion process between the polymer and the mucus layer, providing a strong adhesion and then leading to an enhanced drug delivery rate[37]. The swelling behavior of chitosan, TMC and 4-CBS-TMC flims was observed in pH 1.2, pH 4, pH 5.5 and pH 6.4 (Fig. 6a).

Fig. 6 (a) Swelling behaviors of the chitosan, TMC and 4-CBS-TMC in simulated gastric fluid (SGF, pH 1.2), 0.1 N simulated duodenum buffer (SDF, pH 4.0), 0.1 N phosphate buffer (PB, pH 5.5), simulated jejunum fluid (SJF, pH 6.4), simulated ileum fluid (SIF, pH 7.4) and water. (b) The component of mucoadhesion (cps) of chitosan, TMC, 4-CBS-TMC and SA-4-CBS-TMC in SGF, pH 1.2 and PB, pH 5.5. Data are shown as the mean $\pm$ 1 SD and are derived from three independent repeats.

In the acidic medium (SGF, SDF, PB and SJF) within 6 h of immersion, the TMC and 4-CBS-TMC swelled about 2.28, 2.69, 2.36 and 3.50-folds and 5.11, 6.00, 4.93 and 10.66-folds of the chitosan. The degree of swelling of all samples were significantly higher in acidic medium than in pH 7.4 and water, due to the $-NH_2$ groups being protonated ($-NH_3^+$) at pH < 6.5-6.7[38]. After that the hydrogen bonds were dissociated and induced the network to become loose leading to an increased degree of swelling[39]. TMC provided larger swelling ratio than chitosan owing to the repulsive force among the positive charge of quarternized chitosan backbone. In case of 4-CBS-TMC, excluding the repulsive force of positive charge, 4-CBS substituents prevented the intermolecular interactions between the $-NH_2$ groups of chitosan which affected higher swelling ratio than that of chitosan and TMC.

The swelling behavior of all samples in SIF and water was not clearly difference, but lower than that seen in acidic media. They revealed only about 15% - 20% swelling ratio. In case of SJF and SIF could be explained by the deprotonation of amino group in chitosan backbone. The $-NH_3^+$ groups of chitosan were uncharged leading to a re-association of the hydrogen bonds and, consequently, weaker interactions between the polymer chains and reduced degree of swelling. In water, it mainly depended on the difference in the osmotic pressure inside and outside of the chitosan specimen[40]. Therefore, more water could penetrate into the polymeric networks to increase the degree of swelling.

3.3 Mucoadhesive properties

Chitosan, TMC, 4-CBS-TMC and SA-4-CBS-TMC were investigated and received considerable attention as mucoadhesive polymer based on the viscometric changes of porcine gastric mucin and polymers in both SGF and PB buffer. Because of at a pH of above 6, chitosan becomes deprotonated and losses its charge and so becomes insoluble[41]. Mucoadhesion governed the increased localization and residence time at the site of drug absorption. Moreover, it provided an intensified contact with the mucosa and, subsequently, increased the drug concentration gradient at the required site[42].

The mucoadhesion of chitosan, TMC 4-CBS-TMC and SA-4-CBS-TMC in SGF and PB were summarized in Fig. 6b. In SGF, chitosan showed a component of mucoadhesion of 37.3 cps, while the TMC showed lower component of mucoadhesion (27.4 cps), than that for chitosan. In SGF, the amine ($-NH_2$) groups of chitosan were partially protonated to the ammonium cation ($-NH_3^+$) because

pK_a of chitosan was 5.6. It was not completely interact with negative charge of native mucin (pK_a =2.6). However, it displayed higher the component of mucoadhesion than TMC. The high degree of quaternization may be decreased the mucoadhesive properties. It was explained by changes in the conformation of the respective TMC polymer due to interactions between the fixed positive charges on C-2 position[42]. In case of 4-CBS-TMC, it showed only slightly higher mucoadhesive component at 42.48 cps than chitosan. The mucoadhesive forces were likely to be dominated by electronic interactions and hydrophobic effects of the $-CH_3$ and aromatic part of 4-CBS groups on the polymer backbone that interact with the $-CH_3$ groups on the mucin side chains.

In PB, the 4-CBS-TMC and TMC revealed significantly higher components of mucoadhesiveness than chitosan for 1.74 folds and 1.89 folds, respectively. The mucoadhesive property of all polymers in PB at pH 5.5 was higher than that in SGF at pH 1.2. Because the amino group of all polymers preformed the good dissociation in pH 5.5, the ionic interaction with the anionic form of the sialic acid of mucin was preferred. Moreover, the hydrophobic effect caused the higher mucoadhesive force of 4-CBS-TMC than TMC.

On the other hand, the mucoadhesion of SA-4-CBS-TMC after re-dispersed in SGF and PB exhibited significantly higher mucoadhesive properties than that of the native chitosan. As very high content of SA substituent increased the hydrophobic part, the mucoadhesive properties and viscosity of the mixture increases. Therefore, the mucoadhesion is typically related to the mucoadhesive force between the interacting polymer and the mucin.

4. Conclusions

In summary, SA-4-CBS-TMC nanofibers were easily synthesized by re-dispersion in distilled water while controlling the chemical functionality of 4-CBS and the amino groups of the chitosan backbone on the fiber surfaces. This polymer exhibited suitable swelling and favourable mucoadhesion with the mucus membrane. Therefore, this polymer could be useful in nanotechnology applications, such as drug delivery.

Acknowledgements

References

[a] Program of Petrochemistry, Faculty of Science, Chulalongkorn University, Bangkok, 10330, Thailand
[b] Department of Biology, Faculty of Science, Srinakarinwirot University, Bangkok, 10110, Thailand
[c] Bioorganic Chemistry and Biomaterials Research group, Department of Chemistry, Faculty of Science, Chulalongkorn University, Bangkok, 10330, Thailand
* To whom correspondences should be addressed: nongnuj.j@chula.ac.th

1. D. Ciechanshka, *Fibers Text. East. Eur.*, 2004, **12**, 69-72.
2. K. V. H. Prashanth and R. N. Tharanathan, *Trends Food Sci. Tech.*, 2007, **18**, 117-131.
3. L. Feng, S. Li, H. Li, J. Zhai J, Y. Song, L. Jiang and D. Zhu, *Angew. Chem. Int.*, 2002, **41(7)**, 1221-1223.
4. C. R. Martin, *Chem. Mater.*, 1996, **8**, 1739-1746.
5. P. X. Ma and R. Zhang, *J. Biomed. Mat. Res.*, 1999, **46**, 60-72.
6. J. M. Deitzel, J. Kleinmeyer, J. K. Hirvonen and T. N. C. Beck, *Polymer*, 2001, **42**, 8163-8170.

7. G. J. Liu, J. F. Ding, L. J. Qiao, A. Guo, B. P. Dymov, J. T. Gleeson, T. Hashimoto and K. Saijo, *Chem.-A. European J.*, 1999, **5**, 2740-2749.
8. G. M. Whitesides and B. Grzybowski, *Science*, 2002, **295**, 2418-2421.
9. Z.-M. Huang, Y.-Z. Zhang, M. Kotaki and S. Ramakrishna, *Compos. Sci. Technol.*, 2003, **63**, 2223-22253.
10. H. Homayoni, S. A. H. Ravandi and M. Valizadeh, *Carbohyd. Polym.*, 2009, **77**, 656-661.
11. B. Duan, C. H. Dong, X. Y. Yuan and K. D. Yao, *J. Biomat. Sci.-Polym. E.*, 2004, **15**, 797-811.
12. N. Bhattarai, D. Edmondson, O. Veiseh, F. A. Matsen and M. Zhang, *Biomaterials*, 2005, **26**, 6176-6184.
13. X. Geng, O.-H. Kwon and J. Jang, *Biomaterials*, 2005, **26,** 5427-5432.
14. H. Gan, Y. Li, H. Liu, S. Wang, C. Li, M. Yuan, X. Liu, C. Wang, L. Jiang and D. Zhu, *Biomacromolecules*, 2007, **8**, 1723-1729.
15. K. L. Niece, J. D. Hartgerink, J. J. J. M. Donners and S. I. Stupp, *Am. Chem. Soc.*, 2003, **125**, 7146-7147.
16. J. D. Hartgerink, E. Beniash and S. I. Stupp, *Science*, 2001, **294**, 1684-1688.
17. S. Paramonov, H.-W. Jun and J.D. Hartgerink, *J. Am. Chem. Soc.*, 2006, **128(2)**, 7291-7298.
18. E. Beniash, J. D. Hartgerink, H. Storrie, J. C. Stendahl and S. I. Stupp, *Acta Biomaterialia*, 2005, **1**, 387-397.
19. I. A. Sogias, A. C. Williams and V. V. Khutoryanskiy, *Biomacromolecules*, 2008, **9**, 1837-1842.
20. S. Amir, S. A. Hashim Ali and N. S. B. Mohamed, *Ionics*, 2011, **17**, 121-125.
21. K. Juntapram, N. Praphairaksit, K. Siralertmukul and N. Muangsin, *Carbohyd. Polym.*, 2012, **87(4)**, 2399-2408.
22. P. Suvannasara, K. Juntapram, N. Praphairaksit, K. Siralertmukul and N. Muangsin, *Carbohyd. Polym.* 2013, **94(1)**, 244-252.
23. D. Zhang, J. Li, S. Chen, T. Li, J. Zhou, X. Cheng and A. Zhang, *Macromol. Chem. Physic.*, 2013, **214**, 370-377.
24. H. Cui, M. J. Webber and S. I. Stupp, *J. Pept. Sci.*, 2010, **94(1)**, 1-18.
25. E. Kokkoil, A. Mardilovich, A. Wedekind, E. L. Rexeisen, A. Gang, and J. A. Craig, *Soft Matter*, 2006, **2**, 1015-1024.
26. Y. Huang, H. Yu, L. Guo and Q. Huang, *J. Phys. Chem. B.*, 2010, **114(23)**, 7719-7726.
27. H. Gan, Y. Li, H. Liu, S. Wang, C. Li, M. Yuan, X. Liu, C. Wang, L. Jiang and D. Zhu, *Biomacromolecules*, 2007, **8**, 1723-1729.
28. P. He, X. Li, M. Deng, T. Chen, and H. Liang, *Soft Matter*, 2010, **6**, 1539-1546.
29. Y. Hu, Y. Wu, J. Cai, Y. Ma, B. Wang, K. Xia and X. He, *Int. J. Mol. Sci.*, 2007, **8**, 1-12.
30. T. A. Witten and L. M. Sander, *Phys. Rev. B*, 1983, **27(9)**, 5686-5697.
31. Z. Ma, G. Zhang, X. Zhai, L. Jin, X. Tang, M. Yang, P. Zheng and W. Wang, *Polymer*, 2013, **49**, 1629-1634.
32. M. Reches and E. Gazit, *Nano Lett.*, 2004, **4**, 581-585.
33. M. Hornof, W. Weyenberg, A. Ludwig and A. Bernkop-Schnurch, *J. Control. Release*, 2003, **89**, 419-428.
34. S. Haider and S.-Y. Park, *J. Membr. Sci.*, 2009, **328**, 90-96.
35. J. C. Stendahl, M. S. Rao, M. O. Guler and S. I. Stupp, *Adv. Funct. Mater.*, 2006, **16(4)**, 499-508.
36. D. Mathiowitz, D. E. Chickering and C. M. Lehr, *Drug and the Pharmaceutical Sciences;* Marcel Dekker: New York, 1990.
37. X. Qu, A. Wirsen and A.-C. Albertsson, *Polymer*, 2000, **41**, 4589-4598.
38. R. Hejazi and M. Amiji, *J. Control. Release*, 2003, **89**, 151-165.
39. T. K. Kim, Y. H. Park, K. J. Kim and C. S. Cho, *Int. J. Pharm.*, 2003, **250**, 371-383.
40. E. K. Sarkyt and B. S. Vladimir, *Langmuir*, 1999, **15**, 4230-4235.
41. C. K. S. Pillai, W. Paul and C. P. Sharma, *Prog. Polym. Sci.*, 2009, **34**, 641-678.
42. D. Synman, J. H. Hamman and A. F. Kotze, *Drug Dev. Ind. Pharm.*, 2003, **29**, 61-69.

(a)
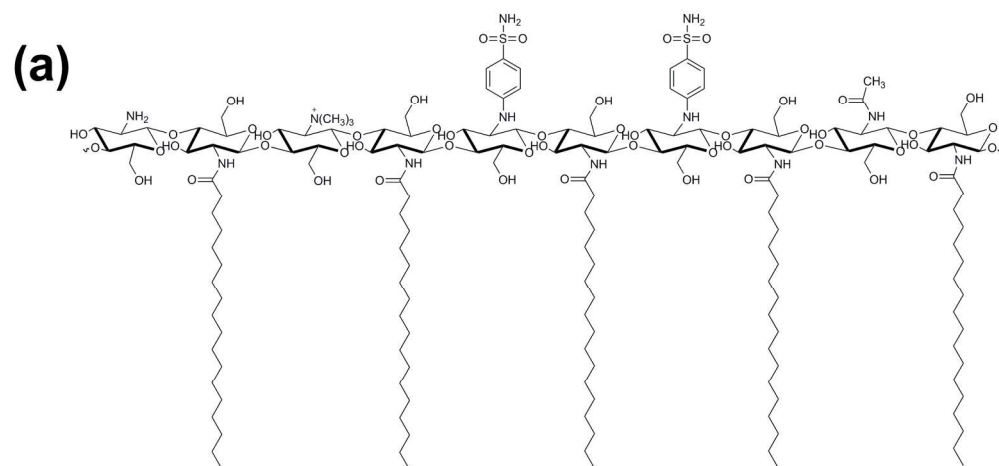
175x81mm (300 x 300 DPI)
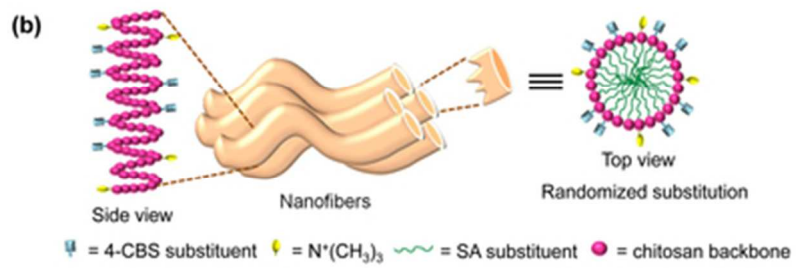
33x11mm (300 x 300 DPI)
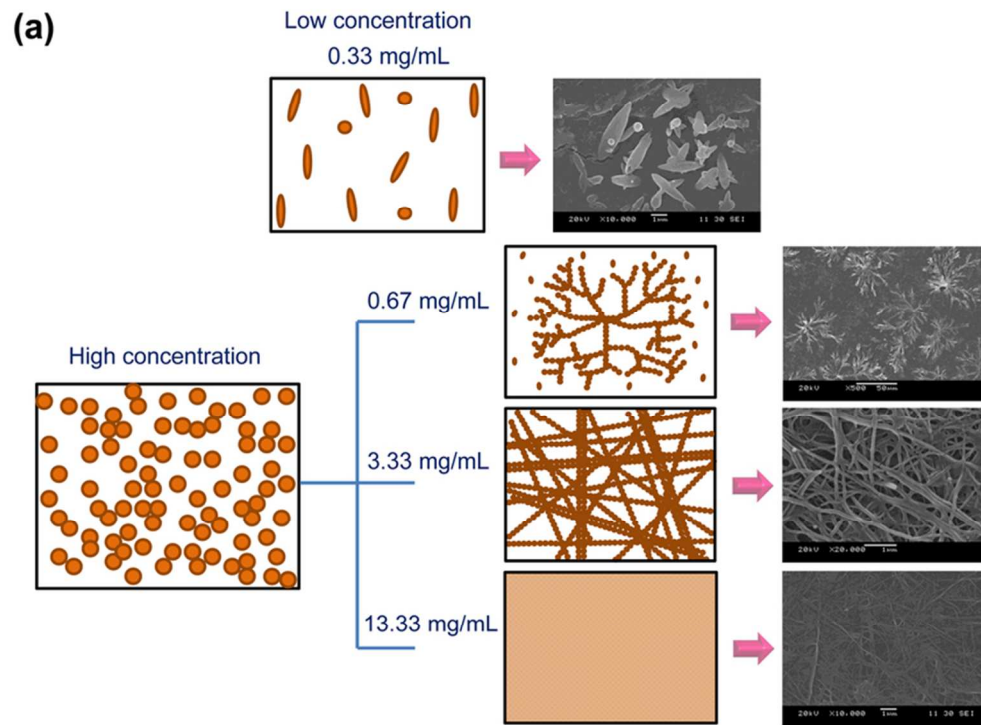
Fig2a
72x53mm (300 x 300 DPI)

(b)

Aggregates of self-assembly

Separate particles on substrate
Time →
Primitive self-assembly
Time →
Self-assembly association

Different morphologies
(Depend on re-dispersed concentration)
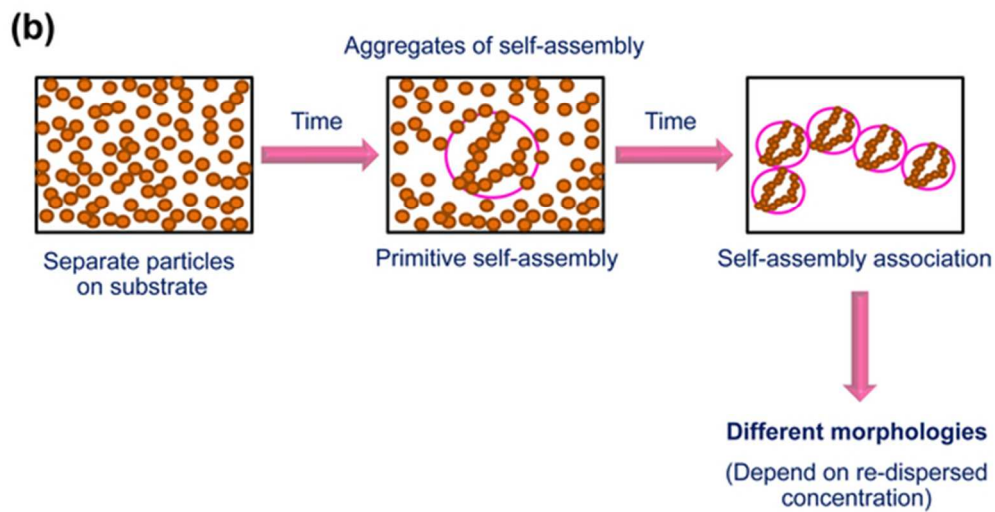
51x27mm (300 x 300 DPI)
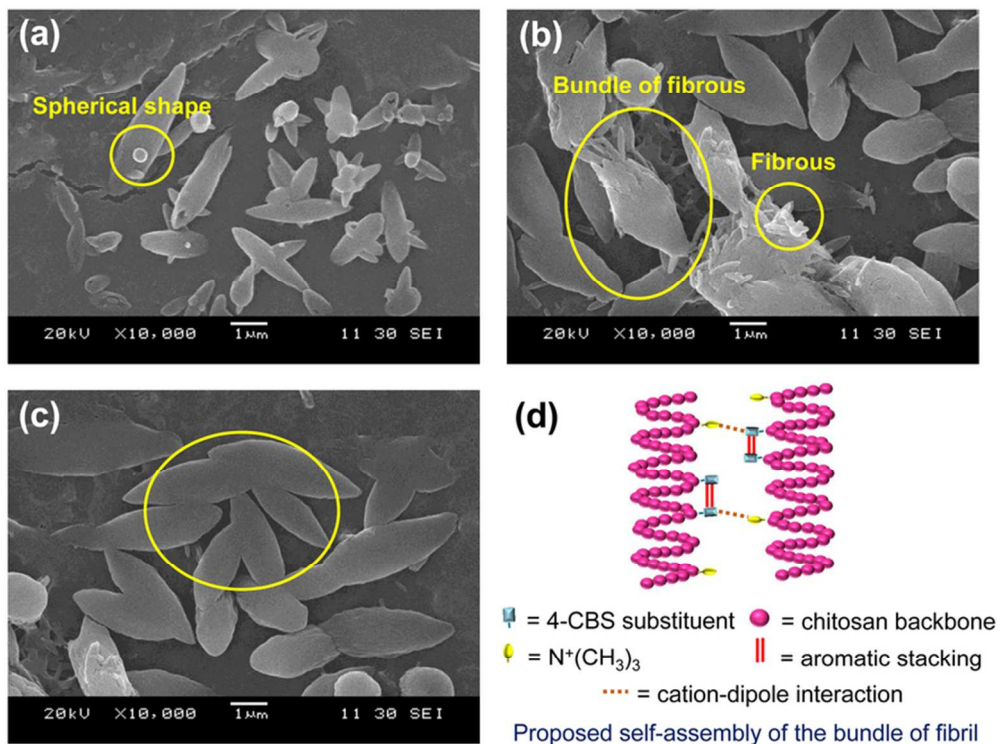
75x56mm (300 x 300 DPI)
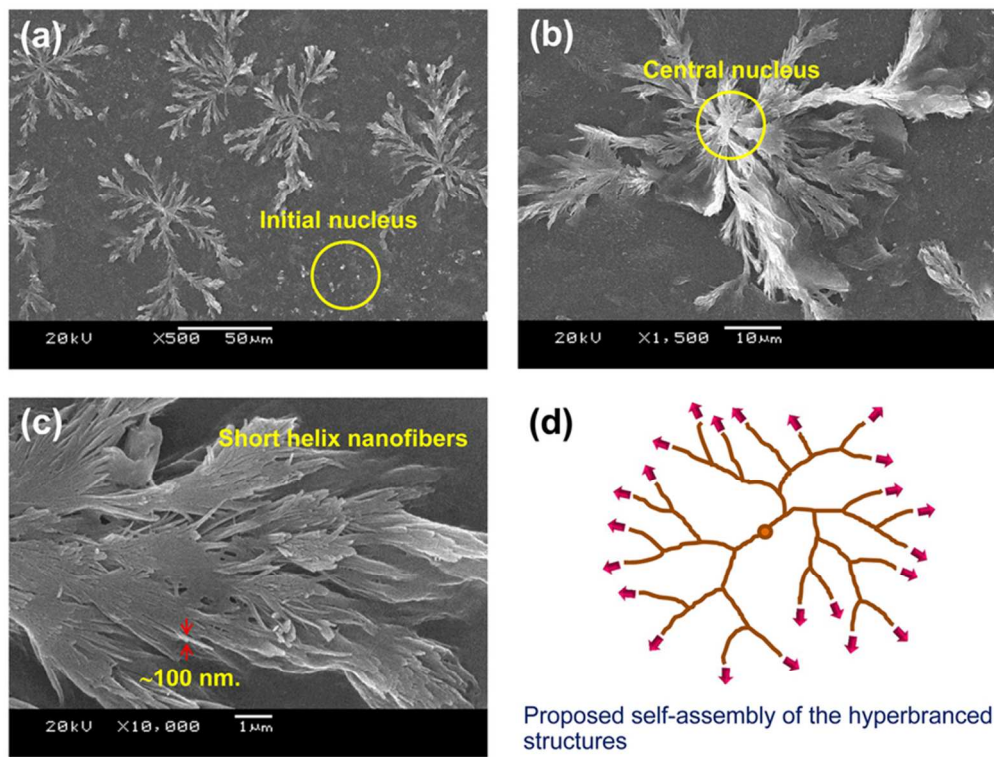
76x57mm (300 x 300 DPI)
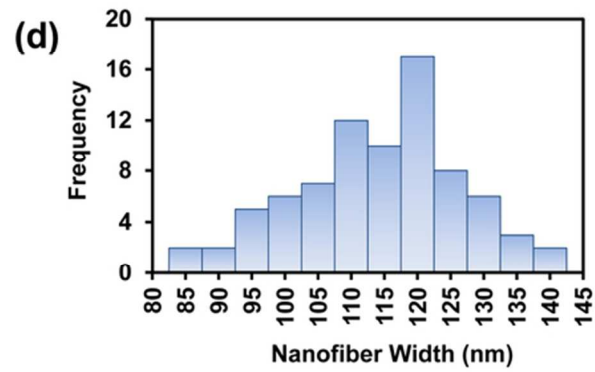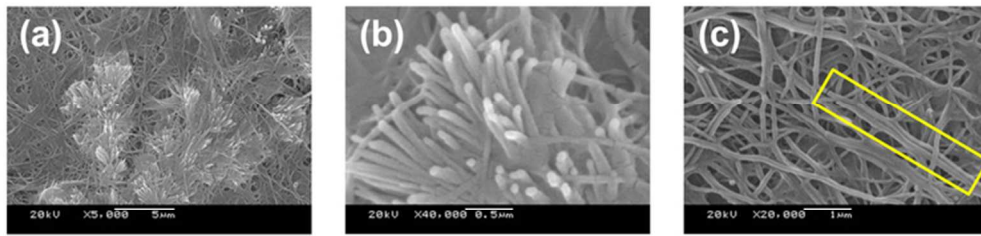
63x40mm (300 x 300 DPI)
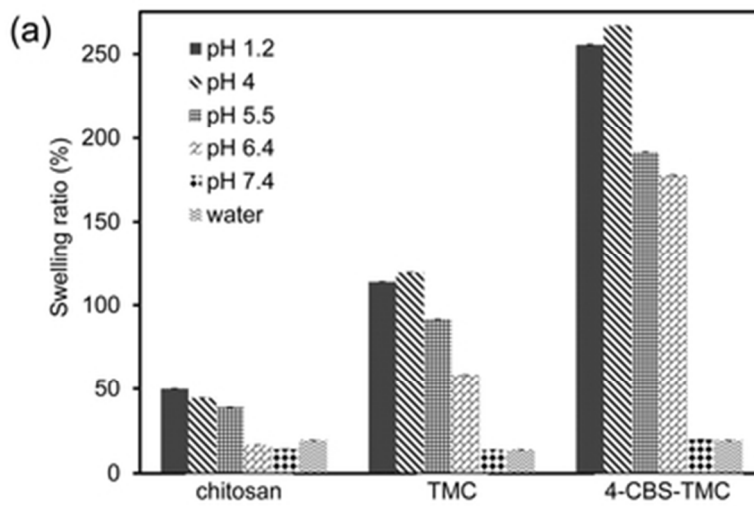
32x21mm (300 x 300 DPI)

31x19mm (300 x 300 DPI)